BMC Biology

RESEARCH ARTICLE

Open Access

Switching of *OAS1* splicing isoforms overcomes SNP-derived vulnerability to SARS-CoV-2 infection

Kei Iida[1,6*†], Masahiko Ajiro[2,7†], Akiko Nakano-Kobayashi[2,3], Yukiko Muramoto[4,5], Toru Takenaga[4,5], Masatsugu Denawa[1], Ryo Kurosawa[2], Takeshi Noda[4,5] and Masatoshi Hagiwara[2*†]

Abstract

Background The SARS-CoV-2 pandemic provided important insights into the relationship between infectious diseases and the human genome. A genomic region encoding the 2′-5′-oligoadenylate synthetase (OAS) family proteins that sense viral genomic RNAs and trigger an antiviral response contains single nucleotide polymorphisms (SNPs) associated with SARS-CoV-2 infection susceptibility. A high-risk SNP identified at the splice acceptor site of *OAS1* exon 6—a terminal exon—alters the proportion of various splicing isoforms of *OAS1* and its activity. However, the actual causality of this SNP or splicing to infection susceptibility remains unknown.

Results In this study, it was found that serine–arginine-rich splicing factor 6 (SRSF6) binds to the splice donor site of the human *OAS1* exon 5. SRSF6 determines the selected alternative terminal exon when the risk allele disrupts the splice acceptor site. Subsequently, an inhibitor for CDC-like kinase was rationally selected as a candidate splicing modulator. RNA-Seq and RT-PCR analyses revealed that this inhibitor can induce splice switching of *OAS1* mRNAs in the human lung adenocarcinoma cell line Calu-3. Under the inhibitor treatment, the cells exhibited reduced SARS-CoV-2 infection rates. Meanwhile, the colonic epithelial cell line Caco-2 expressed non-risk type *OAS1* mRNA isoforms that did not undergo splice-switching or demonstrate altered SARS-CoV-2 sensitivity following treatment with the inhibitor.

Conclusions These results indicate that a high-risk SNP in *OAS1* influences cell susceptibility to SARS-CoV-2 infection by inducing splice-switching at its terminal exon. Additionally, chemical splicing modifiers may prove beneficial in overcoming this genomic vulnerability.

Keywords SARS-CoV-2, Innate immunity, RNA splicing, Small chemical compound, OAS1, SRSF6

†Kei Iida and Masahiko Ajiro share the first authorship.

†Kei Iida and Masatoshi Hagiwara share the last authorship.

*Correspondence:
Kei Iida
iida.kei.3r@kyoto-u.ac.jp
Masatoshi Hagiwara
hagiwara.masatoshi.8c@kyoto-u.ac.jp
[1] Medical Research Support Center, Graduate School of Medicine, Kyoto University Yoshida-Konoe-Cho, Sakyo-Ku, Kyoto 606-8501, Japan
[2] Department of Drug Discovery Medicine, Graduate School of Medicine, Kyoto University Yoshida-Konoe-Cho, Sakyo-Ku, Kyoto 606-8501, Japan
[3] Laboratory of Tumor Tissue Response, Graduate School of Medicine, Kyoto University, 53 Shogoin-Kawahara-Cho, Sakyo-Ku, Kyoto 606-8507, Japan
[4] Laboratory of Ultrastructural Virology, Institute for Life and Medical Sciences, Kyoto University, Kyoto 606-8507, Japan
[5] CREST, Japan Science and Technology Agency, 4-1-8 Honcho, Kawaguchi, Saitama 332-0012, Japan
[6] Present address: Faculty of Science and Engineering, Kindai University, 3-4-1 Kowakae, Higashi-Osaka, Osaka 577-8502, Japan
[7] Present address: Division of Cancer RNA Research, National Cancer Center Research Institute, Tokyo 104-0045, Japan

Background

As of December 2023, more than 770 million people were infected with severe acute respiratory syndrome coronavirus 2 (SARS-CoV-2), with more than 6.9 million recorded deaths due to coronavirus disease 2019 (COVID-19) [1]. At this point, as we begin to overcome this virus through the development of herd immunity and vaccination, it is important to understand the risk of the severe disease caused by polymorphisms among individual genome sequences and continue research on ways to overcome this risk. A previous genome-wide association study (GWAS) comprising more than 2000 patients with COVID-19 uncovered several susceptibility-associated genes, including *LZTFL1*, *CCHCR1*, *OAS1*, *OAS2*, *OAS3*, *DPP9*, *TYK2*, and *IFNAR2* [2]. Similar findings have been reported by the COVID-19 Host Genetics Initiative, which has collected genetic information on over 30 000 patients with COVID-19, including more than 5000 with very severe respiratory symptoms [3]. The GWAS also revealed 131 SNPs associated with severe respiratory conditions ($p < 5 \times 10^{-8}$) in the *OAS1/2/3* gene cluster (Fig. 1a): 5 SNPs within the *OAS1* locus; 72 SNPs within intergenic regions across *OAS1*, *OAS2*, and *OAS3*; 46 SNPs within the *OAS3* locus; and 8 SNPs within the *OAS2* locus. The odds ratios for symptoms associated with these loci reached 1.2, which is notable considering the continued spread of the virus. The importance of the *OAS* family of genes to SARS-CoV-2 infection

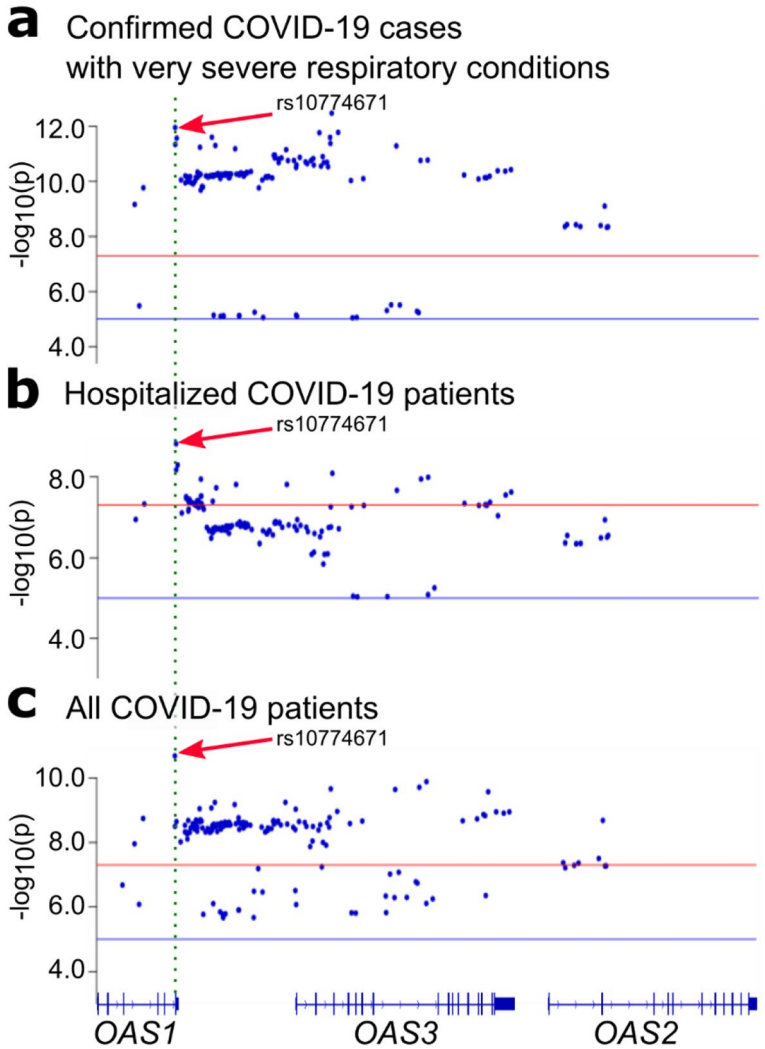

Fig. 1 *OAS1–3* loci possess COVID-19-associated SNPs and respond to SARS-CoV-2. Positions and GWAS *p*-values for SNPs at the *OAS1*, *OAS3*, and *OAS2* loci. GWAS results of confirmed COVID-19 cases with very severe respiratory conditions (a), hospitalized patients with COVID-19 (b), and all patients with COVID-19 (c) (reported by COVID-19 Host Genome Initiative groups). Red and blue horizontal lines show the *p*-value positions of 5E-8 and 1E-5, respectively. The position of rs10774671 SNP is shown with a green dotted line and red arrows

was further demonstrated in an in vitro transcriptomic study of SARS-CoV-2 infection [4]; normal human bronchial epithelial (NHBE) cells exhibited upregulated *OAS1*, *OAS2*, and *OAS3* expression (2.3-, 2.1-, and 2.2-fold increases, respectively). These associated SNPs are concentrated around the terminal exon of *OAS1* and intron 2 of *OAS3;* some were associated with hospitalized patients with COVID-19 (32 SNPs) and others with all patients with COVID-19 (125 SNPs; $p < 5 \times 10^{-8}$; Fig. 1b, c). Among them, the SNP with the lowest *p*-value was the G > A SNP rs10774671 at the last base of *OAS1* intron 5 (Table 1). This SNP is reportedly associated with various infectious viruses, including SARS and dengue virus [5–7].

The objective of this study was to elucidate the molecular mechanisms underlying the effects of SNPs on SARS-CoV-2 infection of human cells. Additionally, potential inhibitors were screened as candidates to protect individuals carrying high-risk SNPs from severe SARS-CoV-2 infection.

Results

OAS1 splice variant regulation by SRSF6

The rs10774671 A/G SNP controls the production of *OAS1* splice variants [8–11]. The G allele of rs10774671 creates the AG-dinucleotide essential for recognizing the exon 6 splice acceptor site for *p46* variant production. The A allele of rs10774671 leads to the alternative splicing of *OAS1* pre-mRNA to produce the *p42*, *p48*, *p44a*, and *p44b* variants [8] (Fig. 2a). OAS1 senses the double-stranded RNA structure, including RNA duplication intermediates of SARS-CoV-2 [12, 13], to synthesize 2′-5′-oligoadenylates, which trigger the activation of latent ribonuclease L (RNase L) for viral RNA degradation [12, 13]. The catalytic activity of OAS1 varies with its splice variants; p46, the major OAS1 isoform produced in the presence of the G allele, presents optimal activity, whereas *p42*, the major isoform produced in the presence of the A allele, exhibits poor activity [14, 15].

In individuals with the A allele, disruption of the exon 6 splice acceptor site induces *OAS1* alternative splicing, yielding *p44a*, *p44b*, and *p48* by activating acceptor sites downstream of exon 5 and *p42* by failing to recognize the exon 5 donor site (Fig. 2a). Assuming that the splice shift from the inactive *p42* to the other variants improves the immune response that is weakened due to the presence of the *OAS1* A allele, the mechanism by which the *p42* variant is dominantly produced was investigated. While searching for splice motifs surrounding the *OAS1* exon 5 donor sites with the ESEfinder tool [16], a binding motif for serine–arginine-rich splicing factor 6 (SRSF6) (5′-UGCUUC-3′) was observed immediately downstream of the exon 5 donor site (Fig. 2b). Accordingly, it was hypothesized that the interaction of SRSF6 with this site prevents U1snRNP from binding to the exon 5 donor site. To test this hypothesis, siRNA-mediated knockdown of *SRSF6* was performed in Calu-3 cells. The subsequent RNA pull-down assay with the exon 5 donor RNA sequence confirmed that U1-70 k binding was promoted when SRSF6 was absent (Fig. 2c).

A pan-CLK inhibitor CaNDY was then applied to dissociate SRSF6 from RNA by preventing CLK-dependent phosphorylation of the SRSF6 RS domain [17], and an RNA pull-down assay was performed with the *OAS1* exon 5 donor sequence. Consistent with the effect of *SRSF6* knockdown (Fig. 2c), CaNDY-treated Calu-3 cells showed more association of U1-70 k with the exon 5 donor sequence, indicating binding of U1snRNP to the site (Fig. 2d). These data indicate that SRSF6 and U1snRNP compete for binding to the *OAS1* exon 5 donor site.

CaNDY induces splice shift in the A allele

To investigate the effect of CLK inhibition on *OAS1* mRNA alternative splicing with the A allele, Calu-3 cells—lung adenocarcinoma cells homozygous for the *OAS1* A allele (Additional file 1: Fig. S1a) [4, 16, 18–21]—were treated with 10 μM CaNDY or DMSO and analyzed for *OAS1* splicing profiles. The RNA-Seq results revealed that CLK inhibition induced splice-switching for *OAS1* with the A allele, suppressing *p42* splicing by 51% and promoting *p44a* splicing by 130% (Fig. 3a, b). The *p44b* isoform was also promoted, but its expression

Table 1 SNPs at the *OAS1* locus associated with confirmed COVID-19 cases with very severe respiratory conditions ($p < 5 \times 10^{-8}$)

Chr	Pos	ID	*p*-value*	log (Odds Ratio)*	Ref	Alt	Location to OAS1 transcript variant 1 (p46)
12	112,912,991	rs2057778	6.86×10^{-10}	0.17	G	T	Intron 3 (1756th base of 5273 nt.)
12	112,914,354	rs4767023	1.70×10^{-10}	0.17	T	C	Intron 3 (3119th base of 5273 nt)
12	112,919,388	rs10774671	1.10×10^{-12}	0.18	G	A	Intron 5 (1688th base of 1688 nt)
12	112,919,404	rs1131476	4.54×10^{-12}	0.18	G	A	Exon 6 (16th base of 515 nt, CDS, Ala > Thr)
12	112,919,637	rs2660	2.68×10^{-12}	0.19	G	A	Exon 6 (249th base of 515 nt, 3′ UTR)

* From GWAS of confirmed COVID-19 cases with very severe respiratory conditions

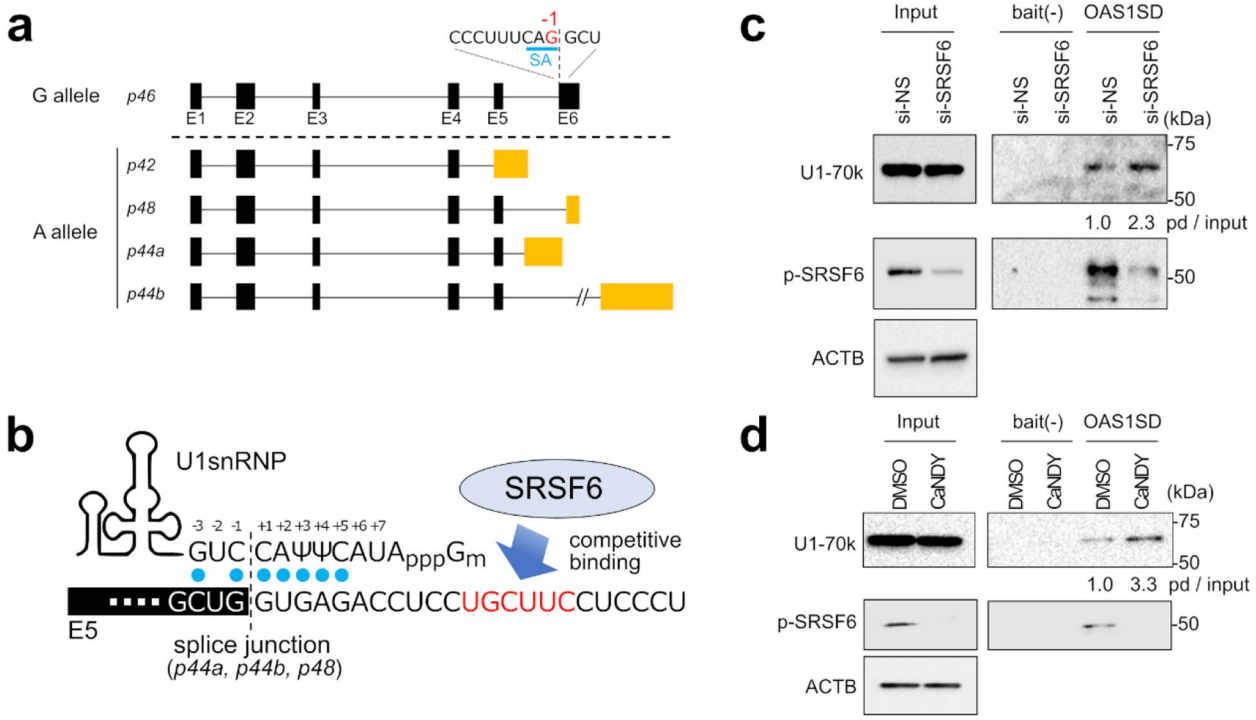

Fig. 2 CLK inhibitor CaNDY induces splice-switching in the *OAS1* rs10774671 A allele. **a** Allele-dependent *OAS1* alternative splicing. Pre-mRNA of *OAS1*, with the rs10774671 G allele at -1 position of exon 6 splice acceptor (SA), dominantly produces the *p46* variant; the A allele leads to alternative splicing to produce the *p42*, *p48*, *p44a*, and *p44b* variants with differences in the last exon (yellow boxes). **b** SRSF6-binding motif (red letters) near the U1-binding site of the *OAS1* donor site for *p44a/p44b/p48* splicing. Blue dots: U1snRNA pairing. **c** Western blotting of U1-70 k and phosphorylated SRSF6 (p-SRSF6) for RNA pull-down products of the *OAS1* exon 5 splice donor (SD) sequence in si-non-specific targets (NS) and si-SRSF6 Calu-3 cells. Input, input samples; bait (-), negative control products without the bait RNA oligo. ACTB served as a loading control. **d** Western blotting of U1-70 k and p-SRSF6 for the RNA pull-down products of the *OAS1* exon 5 SD sequence in Calu-3 cells treated with 0.1% DMSO or 10 μM CaNDY. Captions are the same as in Fig. 2c

remained subtle (Fig. 3a). This observation is consistent with the model suggested by the RNA pull-down assay, wherein the exon 5 donor site is made available for U1snRNP binding upon functional suppression of SRSF6. *OAS1* splice-switching was confirmed by RT-PCR analysis of Calu-3 cells treated with 10 μM CaNDY or DMSO, indicating a shift from the *p42* to *p44a* isoform (Fig. 3c). In contrast, the *p42* and *p44a* isoforms were absent in Daudi cells (lymphoma cells homozygous for rs10774671 G) (Fig. 3c, Additional file 1: Fig. S1b), as reported previously [8, 9]. Consistent with the *p42*-to-*p44a* splice-switching with CaNDY treatment in Calu-3 cells, siRNA-mediated knockdown of *SRSF6* induced the splicing shift from *p42* to *p44a* (Fig. 3d). Similar splice-switching of *OAS1* from the *p42* to *p44a* isoform was observed following treatment of cells with other CLK inhibitors (i.e., ALGERNON and ALGERNON2 [22, 23]) (Additional file 1: Fig. S2) as under CaNDY treatment.

Introns not fully spliced under DMSO conditions were identified for further validation. When SRSF6-binding sequences were − 10 to + 20 from the 5′ splice sites, increased splice site usage was detected under CaNDY treatments, whereas sites lacking SRSF6 binding sequences exhibited poor activity (Additional file 1: Fig. S3, Additional file 2: Table S1). These results indicate that the CLK-dependent phosphorylation of SRSF6 is responsible for the splicing regulation.

The *OAS1 p44a* isoform is a minor splicing isoform expressed in cells carrying the rs10774671 A allele. [8, 9]. However, the antivirus functions of this isoform have not been well characterized. Meanwhile, the colocalization of OAS1 protein with virus-derived dsRNA is critical to its antivirus functions [24]. Additionally, OAS1 p46 localizes to Golgi, where it can access proliferating viruses [11, 25]. Meanwhile, OAS1 p42 does not localize to Golgi, accounting for its weaker antiviral activity [11]. In the present study, *p44a* co-localized with the Golgi membrane (Pearson's coefficient (r) = 0.71; 95% confidence interval (CI): 0.64–0.78 in 13 cells) in HeLa cells (Fig. 3e, f). This observation further supports that the *OAS1 p44a* isoform exerts functional antiviral activity.

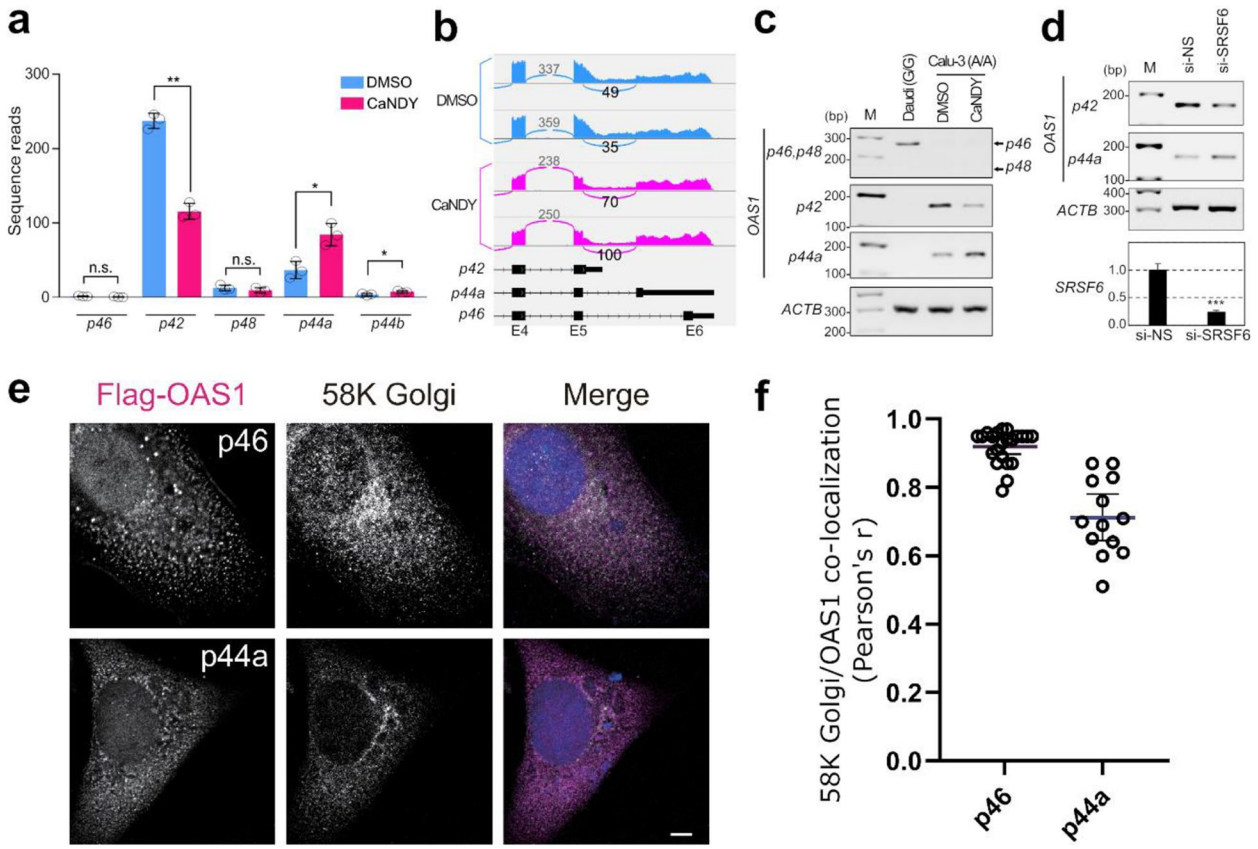

Fig. 3 CLK inhibitor CaNDY induces splice-switching in the *OAS1* rs10774671 A allele. **a** Number of RNA-Seq reads for each *OAS1* splice variant in Calu-3 cells based on the RNA-Seq results. For *p46*, *p48*, *p44a* and *p44b* isoforms, splice-junction reads for their specific Intron 5 were counts. For *p42* isoform, RNA-Seq read continuously aligned from 3′ of Exon 5 to Intron 5 were counted. Dots, number of repeats; error bars ± SD. n.s. $p \geq 0.05$; *$p < 0.05$; **$p < 0.01$ by two-sided Student's *t*-test. **b** RNA-Seq results indicated by a Sashimi plot for a region covering *p42*, *p44a*, and *p46*, treated with 0.1% DMSO or 10 μM CaNDY for 24 h. **c** RT-PCR for *OAS1* alternative splicing profile in Daudi (G/G allele) and Calu-3 (A/A allele) cells treated with 0.1% DMSO or 10 μM CaNDY for 24 h. *ACTB* served as the loading control. **d** (top panel) RT-PCR for *OAS1* alternative splicing profile in si-NS and si-SRSF6 Calu-3 cells. *ACTB* served as the loading control (bottom panel). Relative expression of *SRSF6* mRNAs on si-NS and si-SRSF6 Calu-3 cells, based on the RT-PCR. **e** Representative images for localization of OAS1 p46 and p44a to Golgi membrane. Immunocytostaining for OAS1 p46 and p44a, with 58 K Golgi protein for Golgi membrane marker and Hoechst33342 for nuclear marker in HeLa cells. Bars, 10 μm. **f** Quantification of OAS1 p46 and p44a colocalization at the Golgi membrane plotted by Pearson's correlation coefficient (Pearson's r). Each point represents one cell; 22 and 13 cells were observed for p46 and p44a, respectively. Long horizontal line, median; short horizontal lines, upper and lower quartiles; whiskers, positions of the furthest data points within 1.5 × interquartile range from upper or lower quartile; n.s. $p \geq 0.05$ by Student's two-tailed *t*-test

Through the RNA-Seq analysis of Calu-3 cells with or without CaNDY treatment, 98 DEGs and DASs (Additional file 2: Tables S2 and S3, and Additional file 1: Fig. S4). Of these, 79 DEGs and 43 DASs were similarly affected in Caco-2 cells. The effects of these transcriptome changes on viral infection are presented in the Discussion.

Splice shifts mitigate SARS-CoV-2 infection

Differences in the SARS-CoV-2 infection rate of Calu-3 cells were evaluated after switching the splicing isoform from *p42* to *p44a*. To sufficiently alter the splicing isoform proportion, cells were pre-treated with CaNDY for 24 h before infection. The virus titer was assayed 2 days post-infection (Fig. 4a). The virus titer decreased from 7.69 to 7.45 [$\log_{10}$(TCID50/mL)] (FC = 0.57) in cells treated with CaNDY (Fig. 4b, Additional file 2: Table S4). Additionally, analysis of RNA-Seq reads derived from SARS-CoV-2 revealed a 0.88-fold reduction in Calu-3 cells treated with CaNDY (Additional file 1: Fig. S5).

RNA degradation products were measured to confirm whether the decreased virus titer was due to *OAS1* splicing isoform switching. If the enzymatic activity of OAS1 increases, the activity of RNase L is also expected to increase. Thus, considering that activated RNase L degrades exogenous host cell RNA molecules and

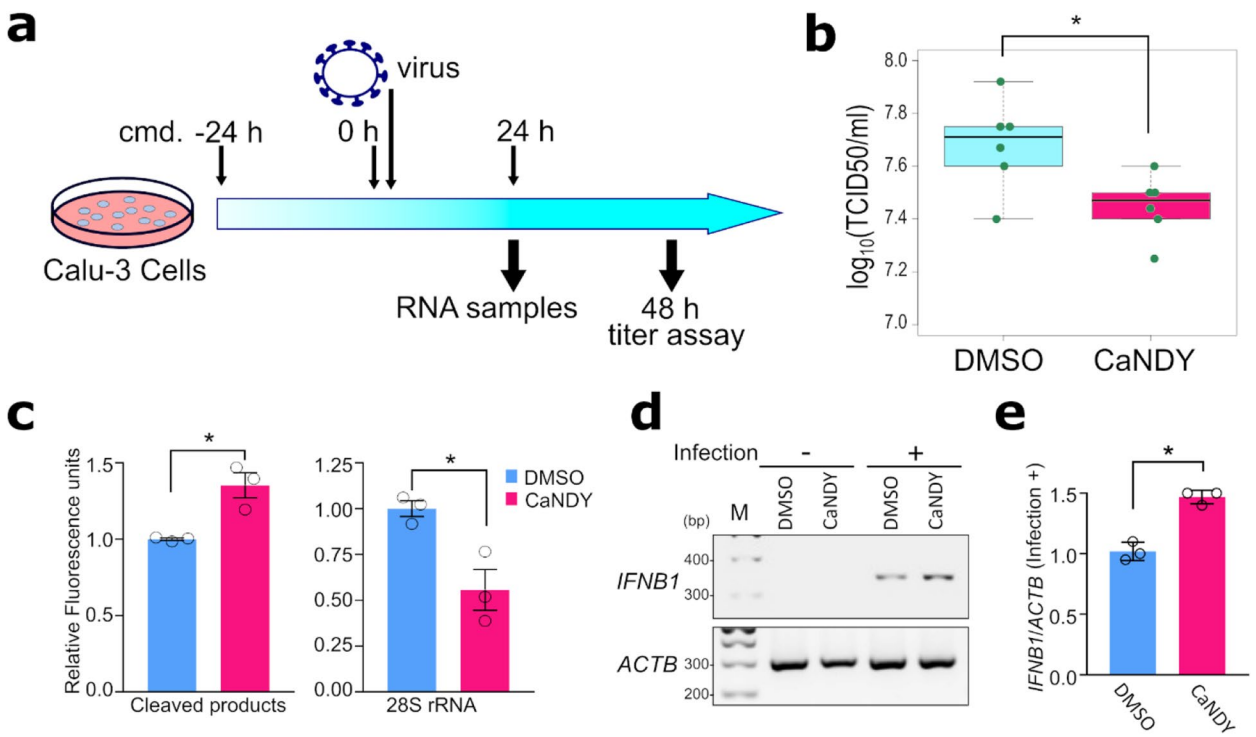

Fig. 4 Calu-3 cells pre-treated with CaNDY mitigated SARS-CoV-2 infection by activating the RNase L and IFN pathways. **a** Scheme for pretreatment with CaNDY before the virus titer assay. **b** Box plots showing logarithm translated virus titers; values are corrected for batch effects (See Methods and Additional file 2: Table S4). Center line, median; box limits, upper and lower quartiles; whiskers, positions of the furthest data points within 1.5 × interquartile range from upper or lower quartiles; $*p < 0.05$ by two-sided Student's *t*-test. **c** Bar plot for cleaved RNA products and 28S rRNA measured using the BioAnalyzer system for the RNA samples from Calu-3 cells, before and after viral infection for 24 h, with and without CaNDY treatments. Error bars, ± SD; $*p < 0.05$ by two-sided Student's *t*-test. **d** RT-PCR results for *IFNB1* mRNA. **e,** Bar plot for quantified IFNB1/ACTB in the infected cells based on the RT-PCR results. Error bars, ± SD; $**p < 0.01$ by two-sided Student's *t*-test

endogenous ribosomal RNAs (rRNAs) [7], rRNA degradation was evaluated to measure RNase L activity. Bands representing degraded rRNA were confirmed in cells infected with SARS-CoV-2 (Fig. 4c). The decomposition product composition (2000–3000 nucleotides) increased slightly (FC = 1.35), with a decrease in the molecular weight and concentration of the 28S rRNA peak (FC = 0.56) upon CaNDY treatment (Fig. 4c, Additional file 1: Fig. S6).

Degraded dsRNA activates interferon (IFN) gene transcription through the OASL- and RIG-I-related pathways [26, 27]. CaNDY treatment increased the transcription of *IFNB1* during viral infection (Fig. 4d, e). Additionally, GSEA for Calu-3 cells treated with CaNDY before SARS-CoV-2 infection revealed an enrichment of a gene set containing upregulated genes in bronchial epithelial cells with interferon β treatments (Gene set ID: M34022, Additional file 1: Fig. S7) [4]. They were consistent with previous studies showing *IFNB1* transactivation during viral infection [28, 29].

To further validate the relationship between the induced production of the *OAS1 p44a* isoform and mitigation of SARS-CoV-2 infection, Calu-3 cells stably overexpressing *OAS1 p44a* were produced (Fig. 5a). The SARS-CoV-2 viral titration assay for *OAS1 p44a*-overexpressing and parental Calu-3 cells revealed a lower virus titer in the cells overexpressing the *OAS1 p44a* isoform (Fig. 5b, from 7.09 to 6.06 [$\log_{10}$(TCID50/mL)]). These results support the importance of CaNDY-induced *OAS1 p44a* for mitigating SARS-CoV-2 infection.

A SARS-CoV-2 infection assay was also performed using human colon adenocarcinoma Caco-2 cells known to be susceptible to SARS-CoV-2 infection [30]. Caco-2 cells harbor more than two copies of chromosome 12 [31] with heterozygosity for rs10774671 A and G alleles, whereas the G allele is predominantly transcribed (> 97%, Additional file 1: Fig. S8a) to produce the *p46* isoform. RNA-Seq revealed that CaNDY treatment did not alter the *p46*-dominant profile of *OAS1* expression in Caco-2 cells (Additional file 1: Fig. S8a). Concordantly, there was no significant difference in SARS-CoV-2 infection with or without CaNDY treatment ($p > 0.05$. Additional file 1: Fig. S8b, DMSO: 3.02, CaNDY: 3.40 [$\log_{10}$ (TCID50/mL)]). These results indicate that CaNDY treatment promotes

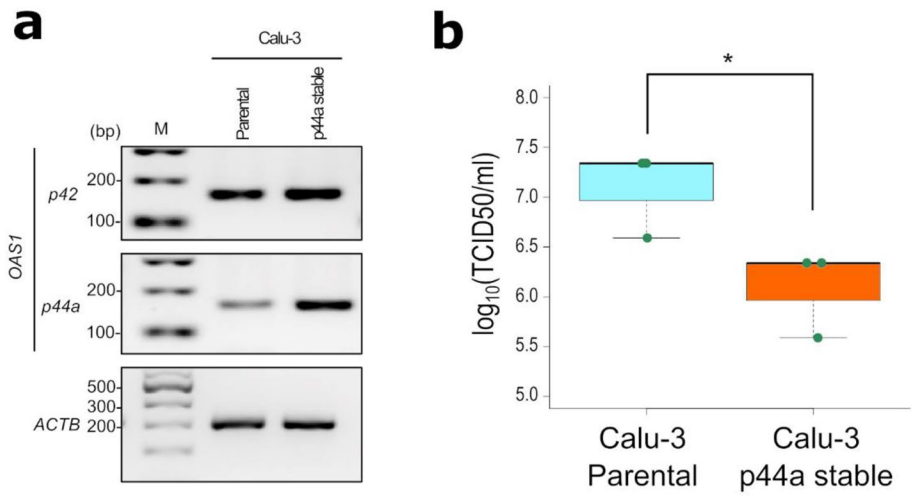

Fig. 5 Calu-3 cells with stable OAS1 p44a isoform expression exhibit mitigated SARS-CoV-2 infection. **a** RT-PCR results for the *p42* and *p44a* isoforms of *OAS1* mRNAs in parental and stably overexpressing the OAS1 *p44a* isoform Calu-3 cells. *ACTB* served as the loading control. **b** Box plots showing logarithm translated virus titers. Center line, median; box limits, upper and lower quartiles; whiskers, 1.5 × interquartile range; *$p < 0.05$ by two-sided Student's *t*-test

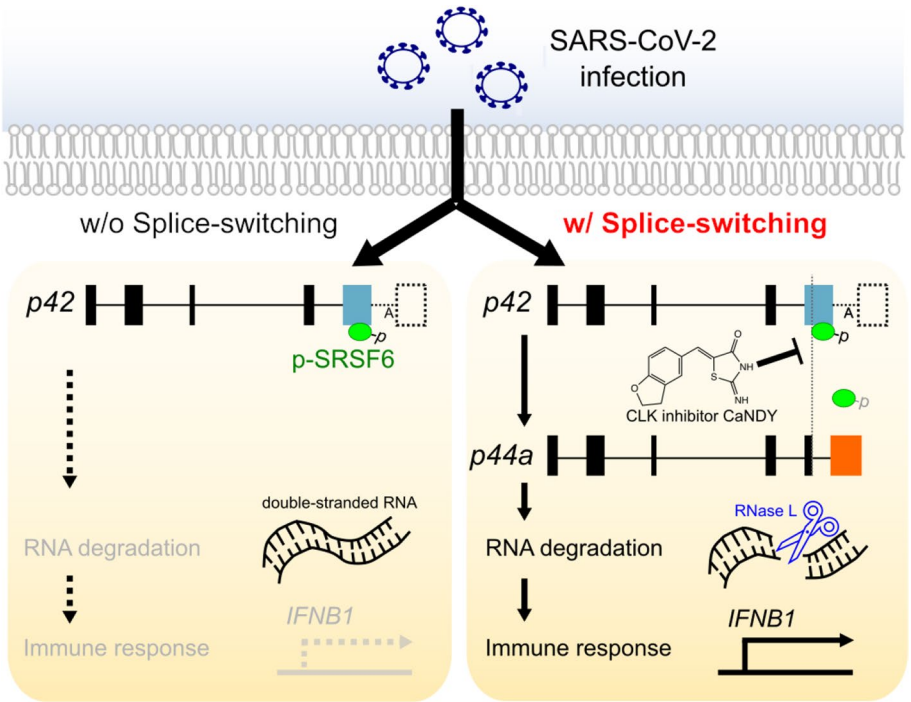

Fig. 6 Graphical summary of this study. In the A allele of *OAS1*, the *p42* isoform is dominantly expressed. Treatment with the CLK inhibitor CaNDY prevents exon 5 splicing donor recognition by functionally inhibiting SRSF6 from binding to the vicinity of the exon 5 splicing donor site. This stimulates splice-switching from *p42* to *p44a*. Enhanced production of the *OAS1 p44a* isoform improves OAS1 activity to increase antiviral responses to SARS-CoV-2

the infection-dependent RNase L pathway and the type I IFN pathway induced by degraded RNAs via splice-switching of *OAS1* isoforms from *p42* to *p44a* in Calu-3 cells (Fig. 6).

Discussion

This study showed that differences in the *OAS1* splicing isoform balance impact the SARS-CoV-2 infectivity of cells by modulating the innate immune response. This suggests that rs10774671 G > A SNP at -1 position of *OAS1* intervening sequence (IVS) 5 that alters the *OAS1* splicing pattern is a causative genetic risk for COVID-19. Although CaNDY treatment did not induce strong viral inhibition, the altered splicing effect of this chemical compound is concentration-dependent [17]. Thus, CaNDY treatment would likely exhibit a similar concentration effect on SARS-CoV-2 infection. Originally, CaNDY was reported as a therapeutic candidate for cystic fibrosis caused by the c.3849 + 10 kb C > T splicing mutation of *CFTR* [17]. In the present study, CaNDY treatment increased the yield of the *p44a* splice isoform, mitigating infection of Calu-3 cells, suggesting that CaNDY treatment overcame A allele-derived vulnerabilities to SARS-CoV-2 infection.

In Caco-2 cells, the SARS-CoV-2 titer was not reduced following pretreatment with CaNDY. This provided insights into the mode of action of CaNDY. More specifically, CaNDY-pretreated Calu-3 and Caco-2 cells shared 79 DEGs and 43 DAS, suggesting that they did not participate in the antiviral effect elicited in Calu-3 cells. Meanwhile, pre-treated Calu-3 and Caco-2 cells exhibit unique switching of the 5′ splice sites of *OAS1* intron 5 due to different SNPs at the OAS1 IVT5-1 position (rs10774671). This further supports the idea that *OAS1* splice-switching is the primary mode of action of CaNDY.

The stability of the p44b splicing isoform is reportedly poor [14, 15]. However, the Calu-3 cells stably expressing p44a in the current study exhibited antiviral potential, indicating that the expressed p44a isoform was functional. The G allele of SNP rs10774671 produces the *p46* splice variant, which possesses 56 amino acids at the C-terminus, compared with the 18 different amino acids present in the *p42* splice variant produced by the A allele (Additional file 1: Fig. S9). This alters OAS1 localization and its interacting partners [9], which may be associated with the differential 2′-5′-oligoadenylate synthesis activities, RNase L activation, and interferon pathway activation. A C-terminal CaaX motif in p46 is required for prenylation and localization to the endomembrane system, including the Golgi apparatus or mitochondria [11, 24, 32]. This localization to the Golgi increases access to proliferating virions. In contrast, the weakened antiviral activity of OAS1 p42 relates to its inability to localize to the Golgi [11, 25]. Although OAS1 p44a lacks the prenylation motif, its C-terminal cysteine is possibly subject to S-palmitoylation. In the case of the D2 dopamine receptor, C-terminal cysteine and S-palmitoylation act as an anterograde signal on the Golgi [33, 34]. In the current study, p44a localized to the Golgi apparatus, resulting in antiviral activity; however, the antiviral activity of p42 and p44a were not directly titrated.

Several clinical trials have evaluated the efficacy of interventions targeting the IFN-β pathway to slow COVID-19 progression [35–37]. The inhibition of the IFN pathway is deemed crucial to prevent cytokine storms in patients with severe COVID-19 [38]. As the rs10774671 SNP can alter the response intensity of the IFN-β pathway, stratification of patients with COVID-19 based on this SNP may inform the selection of appropriate IFN treatments. A recent study by Wickenhagen et al. showed that *OAS1* is an anti-SARS-CoV-2 effector, a gene at the top of the signal transduction cascade starting with the IFN signaling pathway [24]. Moreover, IFN-β overexpression can prevent SARS-CoV-2 infection of human cells [24]. These results support the hypothesis regarding the relationships between OAS1 and IFN-β. However, due to the complexity of the human immune response, reducing the SARS-CoV-2 viral load may not alleviate severe symptoms.

Protective SNPs at the *OAS1/2/3* loci reportedly originated in Neanderthals [39, 40]. Interestingly, rs10774671 A allele, confirmed to be associated with COVID-19 aggravation in this study, was not found in the ancient human genome, the sequenced Neanderthal genome, or the Denisovan genome [41]. This suggests that the G to A mutation at the *OAS1* IVS5-1 position occurred at a relatively modern age in human history. Nevertheless, the rs10774671 A allele has expanded to become a major allele, particularly in Asian populations (Additional file 1: Fig. S10) [21]. This suggests that this variant exerts positive effects on human survival that trade-off with the reduced resistance to viruses.

The current study results indicate that the rs10774671 SNP exacerbates COVID-19 by eliciting changes in the *OAS1* splicing isoform balance. Individuals with the A allele may have a higher risk of SARS-CoV-2 infection and more severe COVID-19 than those with the G allele. However, this genetic risk can be overcome by modulating the splicing phenomenon. Splicing modulation with CaNDY decreased the virus infection rate by 0.56 times in vitro. Changes in the number of susceptible or infected people are simulated for infectious diseases based on the infection rate. If the *OAS1* splicing pattern is altered in individuals carrying the rs10774671 A allele and the immunity of the entire population is boosted, the number of infected individuals should be reduced during peak

infection periods. Hence, combined with SARS-CoV-2 prophylactic vaccines, CaNDY could serve as a protective measure for individuals carrying the rs10774671 A allele.

This study has certain limitations. First, the findings were not confirmed in an in vivo model. Given that this study evaluated the effect of treatment on human-specific SNPs, establishing an animal model will require substantial effort and validation. Additionally, to further elucidate the antiviral mechanism of CaNDY, additional rescue experiments with *RNase L KO* or catalytically dead OAS1 are necessary.

Conclusions

In this study, high-risk *OAS1* SNPs associated with COVID-19 were evaluated in a large-scale GWAS. OAS1 is vital for sensing foreign double-stranded RNAs, including viral RNA genomes. An SNP in the acceptor site of *OAS1* exon 6 alters RNA splicing, which impacts the infectivity of SARS-CoV-2 in human cells. Hence, this change in RNA splicing represents a potential association mechanism between the high-risk SNP and COVID-19. This was further validated by pre-treating cells with a small chemical compound, CaNDY, which inhibits phosphorylation of the splicing factor SRSF6. This resolved the competitive binding of phosphorylated SRSF6 and U1 snRNAs on the donor site of *OAS1* exon 5. Thus, manipulating splicing with a small chemical compound could potentially enhance the resistance to SARS-CoV-2 in individuals with reduced innate immunity due to the presence of the rs10774671 A allele.

Methods

Analysis of GWAS data

GWAS results were obtained from the COVID-19 Host Genetics Initiative database [3]. The following terms were used: "A2_ALL_leave_23andme" for a GWAS of confirmed COVID-19 patients with very severe respiratory conditions vs. population; "B2_ALL_leave_23andme" for a GWAS of hospitalized patients with COVID-19 vs. population; and "C2_ALL_leave_23andme" for a GWAS of all patients with COVID-19 vs. population. Data version 5 was used for all data obtained in this study (January 18, 2021). Sample sizes of 5582, 12 888, and 36 590 individuals were selected for the GWAS datasets of severe respiratory symptoms, hospitalization, and COVID-19 susceptibility, respectively. Sample sizes were determined based on the number of applicable datasets without exclusion.

Cell lines

Daudi cells, derived from Burkitt's lymphoma, were obtained from the cell bank of the National Institutes of Biomedical Innovation, Health and Nutrition (NIBIOHN, Osaka, Japan) and maintained in Roswell Park Memorial Institute (RPMI)-1640 medium (Nacalai Tesque, Kyoto, Japan) supplemented with 20% fetal bovine serum (FBS), 100 U/mL penicillin, and 100 μg/mL streptomycin.

Calu-3 cells, derived from lung adenocarcinoma, were obtained from American Type Culture Collection (ATCC, Manassas, VA, USA) and cultured in Dulbecco's modified Eagle's medium (DMEM; Nacalai Tesque) supplemented with 10% FBS, 100 U/mL penicillin, and 100 μg/mL streptomycin.

Colon adenocarcinoma Caco-2 cells were obtained from ATCC and cultured in DMEM supplemented with 10% FBS, 100 U/mL penicillin, 100 μg/mL streptomycin, and minimum essential media (MEM) non-essential amino acid solution (1×) (Nacalai Tesque).

VeroE6/TMPRSS2 cells were obtained from JCRB Cell Bank and cultured in DMEM (Sigma–Aldrich) supplemented with 10% FBS, 100 U/mL penicillin, and 100 μg/mL streptomycin. All cells were maintained in an incubator at 37 °C with 5% CO_2; mycoplasma was confirmed negative in routine polymerase chain reaction (PCR) tests.

Calu-3 cells stably overexpressing *OAS1 p44a* were prepared by introducing the *OAS1 p44a*-coding sequence with a 3xFLAG amino-terminal attachment into the pAcGFP-N1 vector (Takara Bio) at restriction sites XhoI and NotI (pAM153). Following transfection with Lipofectamine 2000 (Thermo Fisher Scientific), Calu-3 cells were cultured in 10 cm plates with 800 μg/mL G-418-containing media. After 30 days of selection, the resulting colonies were trypsinized and pooled. The cells were stocked as Calu-3 cells stably overexpressing *OAS1 p44a* and used in RT-PCR and infection assays.

siRNA-mediated knockdown of SRSF6

SRSF6 knockdown was conducted as described previously [42]. Briefly, Calu-3 cells at ~ 50% confluence in six-well plates were transfected with siRNAs targeting *SRSF6* (s12741; Thermo Fisher Scientific) or a non-targeting sequence (#4,390,843; Thermo Fisher Scientific) using Lipofectamine RNAi max (Thermo Fisher Scientific)-mediated lipofection with 40 nM siRNA. Cell lysates and total RNA samples were prepared 48 and 72 h after the transfection, respectively.

RNA pull-down assay and western blotting

Calu-3 whole cell lysates were prepared using lysis buffer containing 10 mM Tris–HCl (pH 7.4), 150 mM NaCl, 1 mM ethylenediaminetetraacetic acid, 1% Triton X-100, 0.1% sodium dodecyl sulfate, 0.25% sodium deoxycholate, and 10% glycerol with protease inhibitors (Nacalai Tesque) and phosphatase inhibitors (Sigma–Aldrich, Munich, Germany). They were then sonicated, treated

with DNase I (Promega, Madison, WI, USA) at 37 °C for 5 min, and centrifuged (24 000×*g* at 4 °C for 15 min). The supernatant was used as the soluble fraction for the RNA pull-down assay: 5′-biotin, 3′-dTdT-attached RNA, designed for the sequence adjacent to the *OAS1* exon 5 splice donor (5′-CUGCUGGUGAGACCUCCU GCUUCC-3′, oAM685), was incubated with NeutrAvidin beads (Thermo Fisher Scientific, Waltham, MA, USA) for 2 h at 4 °C (no bait RNA was used for the negative control). The RNA-bound beads were washed with Tris-buffered saline (TBS) thrice and incubated with the Calu-3 cell lysate in the presence of 1% DMSO or 10 μM CaNDY—a CDC-like kinase (CLK) inhibitor [17]—for 16 h with rotation at 4 °C. This was followed by washing thrice with TBS and elution with Laemmli buffer. Three technical replicates for the RNA pull-down assay were independently conducted, three times from a stocked cell lysate.

For western blotting, whole cell lysates or RNA pull-down samples were analyzed using SDS-PAGE with a 4%–20% gradient gel (Bio-Rad, Cat# 4,561,096); the Precision Plus protein standard (Bio-Rad) served as molecular weight marker. Proteins separated via polyacrylamide gel electrophoresis were transferred onto polyvinylidene fluoride (PVDF) membranes and blocked with 5% skim milk in TBS for 60 min at room temperature. Subsequently, membranes were incubated with the following primary antibodies overnight at 4 °C: anti-U1-70 k mouse monoclonal antibody (9C4.1; 05–1588; 1:500; Merk Millipore, Burlington, MA, USA), anti-SR protein (1H4G7) mouse monoclonal antibody (33–9400; 1:200; Thermo Fisher Scientific, Waltham, MA, USA), and anti-β-actin (ACTB) mouse monoclonal antibody (Ac-15; sc-69879; 1:4000; Santa Cruz Biotechnology, Dallas, TX, USA). Membranes were then washed with TBS thrice and incubated with horseradish peroxidase (HRP)-conjugated mouse or rabbit IgG secondary antibodies. Chemiluminescent signals were detected using a ChemiDoc MP Imaging System (Bio-Rad, Hercules, CA, USA).

Transcriptome analysis of CaNDY-treated Calu-3 cells

RNA was extracted from Calu-3 cells using the RNeasy Mini kit (QIAGEN, Hilden, Germany), treated with 10 μM CaNDY or 0.1% dimethyl sulfoxide (DMSO) for 18 h, and used for RNA sequencing (RNA-Seq). Three technical replicates of the total RNA stock were included in the three RNA-Seq assays. RNA-Seq reads were mapped to the human genome sequences (GRCh38) using STAR (ver. 2.7.1a, https://github.com/alexdobin/STAR) with ENCODE options, using the Ensembl genome annotation (ver. 102). Raw reads were counted with bam files, and transcripts per million (TPM) values were calculated using RSEM (ver. 1.2.31, https://github.com/deweylab/RSEM). Differentially expressed genes (DEGs) were identified with DESeq2 (ver. 1.26, https://bioconductor.org/packages/release/bioc/html/DESeq2.html) according to the following criteria: false discovery rate (FDR) < 0.01, absolute $\log_2$ fold change (FC) ≥ 1, TPM ≥ 1, and read counts ≥ 31. Differential alternative splicing (DAS) events were analyzed using a previously described method [43] with the rMATS program (ver. 4.1.1, http://rnaseq-mats.sourceforge.net/rmats4.1.1/) according to the following criteria: FDR < 0.01, read counts ≥ 15, and delta Percent Spliced-In (PSI) ≥ 0.05. The DAS events were compared with the gene annotation data, and the event types were classified as events on the exons constituting the productive mRNAs, events on additional exons/regions of the productive mRNAs, and others.

The Metascape website (https://metascape.org/) was used to characterize the gene set and transcriptome profiles [18]. The same samples were used for RT-PCR.

To assess the relative SARS-CoV-2 RNA expression levels, RNA-Seq data was obtained for Calu-3 cells treated with the virus for 24 h. The RNA-Seq reads were mapped to the combined human genome and SARS-CoV-2 genome database (accession: NC_045512.2); RNA-seq reads uniquely mapped to the SARS-CoV-2 genome were counted.

Immunocytostaining

Full-length OAS1 *p46* and *p44a* coding sequences with an amino-terminal FLAG-tag were subcloned into the pAcGFP-N1 expression vector (Takara Bio. Inc. Shiga, Japan) at XhoI and NotI sites; the resulting vector encodes OAS1 p46 and p44a through the CMV promoter and carries a SV40 polyadenylation signal. HeLa cells cultured in CellCarrier-96 Ultra Microplates (Perkin Elmer, Waltham, USA) were transfected with *OAS1 p46* and *p44a* expression vectors using Lipofectamine 3000 (Thermo Fisher Scientific) for 24 h. Cells were washed with phosphate-buffered saline (PBS) and fixed with 4% paraformaldehyde. Cells were then washed with PBS, permeabilized with 0.1% Triton-X100, washed with PBS, and blocked with 5% normal donkey serum and 3% bovine serum albumin (BSA) in PBS. Subsequently, cells were incubated with anti-58 K Golgi mouse monoclonal (58 K-9, Abcam) and anti-FLAG rabbit polyclonal (Sigma) primary antibodies. They were then incubated with secondary antibodies: anti-rabbit IgG donkey polyclonal with Alexa Fluor 555 (Thermo Fisher Scientific) and anti-mouse IgG donkey polyclonal with Alexa Fluor 647 (Thermo Fisher Scientific). Following nuclear staining with hoechst33342 (Thermo Fisher Scientific), fluorescent images were acquired with an SP8 confocal

microscope (Leica, Wetzler, Germany); colocalization was quantified using Fiji [44].

SARS-CoV-2 infection

SARS-CoV-2 isolate (SARS-CoV-2/Hu/DP/Kng/19–027), kindly provided by the Kanagawa Prefectural Institute of Public Health, was propagated in VeroE6/TMPRSS2 cells [45], which was used as the virus stock after clarification of cell debris. Calu-3 and Caco-2 cells were pre-treated with 10 μM CaNDY or 0.1% DMSO for 24 h, infected with SARS-CoV-2 at a multiplicity of infection (MOI) of 0.01, and maintained in the presence of 10 μM CaNDY or 0.1% DMSO. *OAS1 p44a*-overexpressing Calu-3 and parental Calu-3 cells were infected under the same condition without compound treatment. Virus titers were determined using the 50% tissue culture infectious dose ($TCID_{50}$) with VeroE6/TMPRSS2 cells at 48 h post-infection (pi).

RNA was also extracted from Calu-3 cells treated with CaNDY or DMSO and infected with SARS-CoV-2 at an MOI of 1.0 for 24 h. Titration assays were conducted with six biological replicates for Calu-3 under CaNDY treatment, three for Caco-2 under CaNDY treatment, and three for Calu-3 stably overexpressing *OAS1 p44a*. All experiments with SARS-CoV-2 were performed in a biosafety level 3 containment laboratory at the Institute for Life and Medical Sciences, Kyoto University.

RNA degradation analysis

RNA samples were diluted with RNase-free ultrapure water to 200 ng/μL. The quality of the diluted RNA samples was evaluated using the Agilent RNA 6000 Nano Kit and the Agilent 2100 Bioanalyzer. Three biological replicates from independent cell cultures were prepared for DMSO and CaNDY treatments for the infected cells, respectively. Total RNA from transcriptome analysis represented the uninfected control. The gel-like image produced by the 2100 Bioanalyzer was visualized using 2100 Expert Software (ver. B.02.11, Agilent Technologies) in pseudo colors with default settings. For detailed analyses, the migration time and fluorescence unit data were extracted in CSV format aligned with the sample data. Next, the fluorescence unit values were normalized to an RNA concentration of 300 ng/μL. The data between 43.3 s and 48.0 s of the migration time were selected as cleaved RNA products and between 49.9 s and 51.4 s as the 28S rRNA. The sums of the fluorescence unit values were used for further analysis. The values were scaled to the mean values of DMSO samples to construct bar plots.

RT-PCR and real-time RT-PCR

The total RNA extracted from cultured cells was reverse transcribed using PrimeScript RTase (Takara Bio, Shiga, Japan) with random hexamers; the products were amplified with ExTaq DNA polymerase (Takara Bio) or KOD one (TOYOBO, Osaka, Japan) with target-specific primer sets (Additional file 2: Table S5). The RT-PCR products were detected using the ChemiDoc MP Imaging System (Bio-Rad); subsequent analysis was performed using Image Lab software (Bio-Rad). RT-PCR was conducted in three technical replicates per sample. Real-time RT-PCR was conducted for *SRSF6* (Hs00740177_g1, Thermo Fisher Scientific) and *ACTB* (Hs01060665_g1, Thermo Fisher Scientific), using the TaqMan PCR master mix (Thermo Fisher Scientific) for RT products. Real-time RT-PCR signals were detected using the Step One Plus real-time PCR system (Thermo Fisher Scientific) and analyzed for the relative expression level of *SRSF6* using the $2^{-\Delta\Delta Ct}$ method.

Gene Set Enrichment Analysis

For Gene Set Enrichment Analysis (GSEA), a software version 4.4.3 [19] and a database; the Molecular Signatures Database (MSigDB) version 7.4 were used. RNA-seq profiles were obtained from SARS-Cov-2-infected Calu-3 cells. Target samples (n = 3) were pre-treated with CaNDY, and control samples (n = 3) were not pre-treated. Genes were discarded from this analysis when the TPM value was < 1.0. For ranking the genes, "Diff_of_Classes" method was used.

Abbreviations

OAS	2′-5′-Oligoadenylate synthetase
GWAS	Genome-wide association study
SNP	Single nucleotide polymorphism

Supplementary Information

The online version contains supplementary material available at https://doi.org/10.1186/s12915-025-02173-3.

Additional file 1: Fig. S1. Genotyping of the rs10774671 SNP. Results of SNP genotyping of Calu-3 cells and Daudi cells. Fig. S2. CLK inhibitors affect the OAS1 alternative splicing profile. Fig. S3. Analysis for relationship between SRSF6 binding adjacent to 5′ splice site and enhancement of splice site (SS)-usages under CaNDY treatments. Fig. S4. Pathway analysis for CaNDY-affected genes. Fig. S5. Bar plot for the fraction of RNA fragments derived from SARS-CoV-2, calculated with RNA-seq. Fig. S6. RNA degradation in SARS-CoV-2-infected cells. Fig. S7. A result of Gene Set Enrichment Analysis (GSEA). Fig. S8. CLK inhibitor exerts a non-significant effect on Caco-2 cells. Fig. S9. A multiple alignment of amino acid sequences of OAS1 splicing isoforms. Fig. S10. Allele frequency of the rs10774671 SNP.

Additional file 2: Table S1. Relationship between SRSF6 binding motifs around 5′ splice sites and CaNDY effects for splice site usages. Table S2. Upregulated Genes in CaNDY-treated Calu-3 cells. Table S3. Altered splicing events yielding protein-coding variants in CaNDY-treated Calu-3 cells. Table S4. Raw and Batch-effect corrected results of the virus titer assay. Table 5. List of primers used in this study.

Additional file 3: An archived file containing original gel images for Figs. 2c, 2d, 3c, 3d, 4d, and Additional file 1: Figure S2.

Acknowledgements
We would like to thank Dr. Ken-ichiro Kamei of Kyoto University for technical assistance in the Caco-2 cell study.

Authors' contributions
K.I. conducted bioinformatic analysis. M.A., M.D., R.K., and NK.A. conducted biological experiments with cultured cells. Y.M., T.T., and T.N. conducted viral experiments. K.I., M.A., and M.H. wrote the paper. All authors read and approved the final manuscript.

Funding
This study was supported by grants 15H05721 (to M.H., K.I., and M.A.), 19K07367 (to M.A.), 21H05042 (to M.H. and M.A.), and 20K07310 (to K.I.) from the Japan Society for the Promotion of Science; the Kansai Economic Federation (KANKEIREN) (to M.H.); Research Program on Emerging and Re-emerging Infectious Disease grants JP20fk0108270 (to M.H. and T.N.),JP20ek0109327 (to M.H., and M.A.), and JP20fk0108454 (to M.H.) from AMED; the JST Core Research for Evolutional Science and Technology grant JPMJCR20HA (to T.N.); the Grant for Joint Research Project of the Institute of Medical Science, University of Tokyo; and the Joint Usage/Research Center program of Institute for Frontier Life and Medical Sciences Kyoto University (to T.N.).

Data availability
The datasets generated during and analyzed during the current study are available from the corresponding author upon reasonable request. The original RNA-Seq data have been deposited at the Gene Expression Omnibus (GEO) of the National Center for Biotechnology Information (NCBI) with the accession ID GSE174398, GSE207270, and GSE244026. All codes used in this study are available upon request.

Declarations

Ethics approval and consent to participate
This article does not contain any content that requires ethical approval or consent to participate.

Consent for publication
This article does not contain any content that requires consent for publication.

Competing interests
M.H. is a founder, shareholder, and member of the scientific advisory board of KinoPharma, Inc., and BTB Drug Development Research Center Co., Ltd. This work has been filed for a world patent application (WO2022/255411 A1); M.H., K.I., and T.N. are named as co-inventors. The authors have no other competing interests to declare.

Received: 26 February 2024 Accepted: 27 January 2025
Published online: 03 March 2025

References

1. World Health Organization (WHO) WHO COVID-19 dashboard. https://covid19.who.int. Accessed 10 Jan 2024.
2. Pairo-Castineira E, Clohisey S, Klaric L, et al. Genetic mechanisms of critical illness in COVID-19. Nature. 2021;591:92–8.
3. COVID-19 Host Genetics Initiative. Mapping the human genetic architecture of COVID-19. Nature. 2021;600:472–7.
4. Blanco-Melo D, Nilsson-Payant BE, Liu W, et al. Imbalanced host response to SARS-CoV-2 drives development of COVID-19. Cell. 2020;181:1036-1045.e9.
5. Hamano E, Hijikata M, Itoyama S, et al. Polymorphisms of interferon-inducible genes OAS-1 and MxA associated with SARS in the Vietnamese population. Biochem Biophys Res Commun. 2005;329:1234–9.
6. He J, Feng D, de Vlas SJ, et al. Association of SARS susceptibility with single nucleic acid polymorphisms of OAS1 and MxA genes: a case-control study. BMC Infect Dis. 2006;6:106.
7. Lin R-J, Yu H-P, Chang B-L, Tang W-C, Liao C-L, Lin Y-L. Distinct antiviral roles for human 2',5'-oligoadenylate synthetase family members against dengue virus infection. J Immunol. 2009;183:8035–43.
8. Noguchi S, Hamano E, Matsushita I, Hijikata M, Ito H, Nagase T, Keicho N. Differential effects of a common splice site polymorphism on the generation of OAS1 variants in human bronchial epithelial cells. Hum Immunol. 2013;74:395–401.
9. Kjær KH, Pahus J, Hansen MF, Poulsen JB, Christensen EI, Justesen J, Martensen PM. Mitochondrial localization of the OAS1 p46 isoform associated with a common single nucleotide polymorphism. BMC Cell Biol. 2014;15:1–14.
10. Liu X, Xing H, Gao W, et al. A functional variant in the OAS1 gene is associated with Sjögren's syndrome complicated with HBV infection. Sci Rep. 2017;7:17571.
11. Soveg FW, Schwerk J, Gokhale NS, et al. Endomembrane targeting of human OAS1 p46 augments antiviral activity. Elife. 2021;10:e71047.
12. Schlee M, Hartmann G. Discriminating self from non-self in nucleic acid sensing. Nat Rev Immunol. 2016;16:566–80.
13. Sadler AJ, Williams BRG. Interferon-inducible antiviral effectors. Nat Rev Immunol. 2008;8:559–68.
14. Di H, Elbahesh H, Brinton MA. Characteristics of human OAS1 isoform proteins. Viruses. 2020;12:152.
15. Carey CM, Govande AA, Cooper JM, Hartley MK, Kranzusch PJ, Elde NC. Recurrent loss-of-function mutations reveal costs to OAS1 antiviral activity in primates. Cell Host Microbe. 2019;25:336-343.e4.
16. Cartegni L. ESEfinder: a web resource to identify exonic splicing enhancers. Nucleic Acids Res. 2003;31:3568–71.
17. Shibata S, Ajiro M, Hagiwara M. Mechanism-Based Personalized Medicine for Cystic Fibrosis by Suppressing Pseudo Exon Inclusion. Cell Chem Biol. 2020;27:1472-1482.e6.
18. Tripathi S, Pohl MO, Zhou Y, et al. Meta- and orthogonal integration of influenza "OMICs" data defines a role for UBR4 in virus budding. Cell Host Microbe. 2015;18:723–35.
19. Subramanian A, Tamayo P, Mootha VK, et al. Gene set enrichment analysis: A knowledge-based approach for interpreting genome-wide expression profiles. Proc Natl Acad Sci. 2005;102:15545–50.
20. Madeira F, Madhusoodanan N, Lee J, Eusebi A, Niewielska A, Tivey ARN, Lopez R, Butcher S. The EMBL-EBI Job Dispatcher sequence analysis tools framework in 2024. Nucleic Acids Res. 2024;52:W521–5.
21. Marcus JH, Novembre J. Visualizing the geography of genetic variants. Bioinformatics. 2017;33:594–5.
22. Nakano-Kobayashi A, Awaya T, Kii I, Sumida Y, Okuno Y, Yoshida S, Sumida T, Inoue H, Hosoya T, Hagiwara M. Prenatal neurogenesis induction therapy normalizes brain structure and function in Down syndrome mice. Proc Natl Acad Sci. 2017;114:10268–73.
23 Nakano-Kobayashi A, Fukumoto A, Morizane A, et al. Therapeutics potentiating microglial p21-Nrf2 axis can rescue neurodegeneration caused by neuroinflammation. Sci Adv. 2020;6:eabc1428.
24 Wickenhagen A, Sugrue E, Lytras S, et al. A prenylated dsRNA sensor protects against severe COVID-19. Science. 2021;374:eabj3624.
25. Banday AR, Stanifer ML, Florez-Vargas O, et al. Genetic regulation of OAS1 nonsense-mediated decay underlies association with COVID-19 hospitalization in patients of European and African ancestries. Nat Genet. 2022;54:1103–16.
26. Choi UY, Kang J-S, Hwang YS, Kim Y-J. Oligoadenylate synthase-like (OASL) proteins: dual functions and associations with diseases. Exp Mol Med. 2015;47:e144–e144.
27. Ibsen MS, Gad HH, Andersen LL, Hornung V, Julkunen I, Sarkar SN, Hartmann R. Structural and functional analysis reveals that human OASL binds dsRNA to enhance RIG-I signaling. Nucleic Acids Res. 2015;43:5236–48.
28 Ford E, Thanos D. The transcriptional code of human IFN-β gene expression. Biochim et Biophysa Acta (BBA) - Gene Regul Mech. 2010;1799:328–36.
29. Schwanke H, Stempel M, Brinkmann MM. Of keeping and tipping the balance: host regulation and viral modulation of IRF3-dependent IFNB1 expression. Viruses. 2020;12:733.
30. Hoehl S, Rabenau H, Berger A, et al. Evidence of SARS-CoV-2 infection in returning travelers from Wuhan, China. N Engl J Med. 2020;382:1278–80.
31. Bezrookove V, Smits R, Moeslein G, Fodde R, Tanke HJ, Raap AK, Darroudi F. Premature chromosome condensation revisited: a novel chemical

approach permits efficient cytogenetic analysis of cancers. Genes Chrom Cancer. 2003;38:177–86.
32. Skrivergaard S, Jensen MS, Rolander TB, Nguyen TBN, Bundgaard A, Nejsum LN, Martensen PM. The cellular localization of the p42 and p46 oligoadenylate synthetase 1 isoforms and their impact on mitochondrial respiration. Viruses. 2019;11:1122.
33. Ebersole B, Petko J, Woll M, Murakami S, Sokolina K, Wong V, Stagljar I, Lüscher B, Levenson R. Effect of C-Terminal S-palmitoylation on D2 dopamine receptor trafficking and stability. PLoS ONE. 2015;10:e0140661.
34. Ernst AM, Syed SA, Zaki O, et al. S-Palmitoylation sorts membrane cargo for anterograde transport in the golgi. Dev Cell. 2018;47:479-493.e7.
35. Hung IF-N, Lung K-C, Tso EY-K, et al. Triple combination of interferon beta-1b, lopinavir–ritonavir, and ribavirin in the treatment of patients admitted to hospital with COVID-19: an open-label, randomised, phase 2 trial. The Lancet. 2020;395:1695–704.
36. Shalhoub S. Interferon beta-1b for COVID-19. The Lancet. 2020;395:1670–1.
37. Monk PD, Marsden RJ, Tear VJ, et al. Safety and efficacy of inhaled nebulised interferon beta-1a (SNG001) for treatment of SARS-CoV-2 infection: a randomised, double-blind, placebo-controlled, phase 2 trial. Lancet Respir Med. 2021;9:196–206.
38. Nile SH, Nile A, Qiu J, Li L, Jia X, Kai G. COVID-19: Pathogenesis, cytokine storm and therapeutic potential of interferons. Cytokine Growth Factor Rev. 2020;53:66–70.
39. Zeberg H, Pääbo S. A genomic region associated with protection against severe COVID-19 is inherited from Neandertals. Proc Natl Acad Sci. 2021;118:e2026309118.
40. Zhou S, Butler-Laporte G, Nakanishi T, et al. A Neanderthal OAS1 isoform protects individuals of European ancestry against COVID-19 susceptibility and severity. Nat Med. 2021;27:659–67.
41. Mendez FL, Watkins JC, Hammer MF. Neandertal origin of genetic variation at the cluster of OAS immunity genes. Mol Biol Evol. 2013;30:798–801.
42. Ajiro M, Awaya T, Kim YJ, et al. Therapeutic manipulation of IKBKAP mis-splicing with a small molecule to cure familial dysautonomia. Nat Commun. 2021;12:6039.
43. Sakuma M, Iida K, Hagiwara M. Deciphering targeting rules of splicing modulator compounds: case of TG003. BMC Mol Biol. 2015;16:16.
44. Schindelin J, Arganda-Carreras I, Frise E, et al. Fiji: an open-source platform for biological-image analysis. Nat Methods. 2012;9:676–82.
45. Matsuyama S, Nao N, Shirato K, et al. Enhanced isolation of SARS-CoV-2 by TMPRSS2-expressing cells. Proc Natl Acad Sci. 2020;117:7001–3.

Publisher's Note